The significance of structural parameters in failure of cemented carbides

The Significance Of Structural Parameters In Failure Of Cemented Carbides

H.J.J. Kals , Eindhoven University of Technology; P.J. Gielisse , University of Rhode Island
submitted by
A.C.H. van der Wolf , Eindhoven University of Technology(1)

Summary : Brittle fracture of cemented carbides is an important factor in cutting tool performance. It has been observed that strength and toughness of cemented carbides are predominantly influenced by grain size and layer thickness of the binder. Some investigators have determined a significant dependence of strength on the isostatic-stress component. This dependence was found to increase with decreasing percentage of the binder component. An attempt has been made to evaluate the ratio of the effective stress and the maximum tensile stress component within the binder ($c=\bar{\sigma}/\sigma$) in relation to strength. It has been shown that the ultimate uniaxial tensile strain can be related to c. In turn, the parameter c is dependent on structural parameters. Equations can be derived wich permit the prediction of failure in terms of the ultimate uniaxial strain if the E-value is known. The use of the E-modulus also accounts for the influence of porosity.

I Introduction

It is a wellknown fact that grain size and mean free path between the grains influence strength and toughness of cemented carbides. Gurland and Parikh (see reference [1])) have shown that strength increases with increasing value of the mean free path λ. However, beyond $\lambda \approx 0{,}45$ µm - when the influence of plastic deformation becomes important - the trend is reversed (Fig. 1). Hatano [2]) and Brandes [3]), who examined the influence of the deformation rate and the isostatic-stress component on brittle failure respectively, concluded that the ultimate uniaxial strain (ε_f) rather than the fracture strength (σ_f) is the reliable brittle failure criterion. Brandes showed that brittle failure occurs, - irrespective of the state of stress - when the maximum elastic strain

$$\varepsilon_1 = \frac{1}{E}\{\sigma_1 - \nu(\sigma_2 + \sigma_3)\} \qquad (1)$$

reaches a critical value.
This would mean that the combined principal stresses rather than the maximum uniaxial stress determine failure. It has been shown by Kals and Veenstra [4]) that for a number of representative cutting tool carbides the uniaxial strain in bending (ε_{fT}) appears to be related to the mean free path λ. An attempt to relate the transverse rupture strength (σ_{fT}) to the mean free path was not succesfull. From work of Doi et al. [5]), Fig. 2, it appears that there is a systematic increase in rupture strength with a decrease in grain size. Although a relationship between structural and strength parameters exists, there remains the wish to determine a generally applicable structural parameter which would uniquely quantify the fracture behaviour of cemented carbides. It has been the purpose of the present analysis to contribute towards this objective. Emphasis has been placed on the definition of failure in terms of one easily determinable structural material parameter.

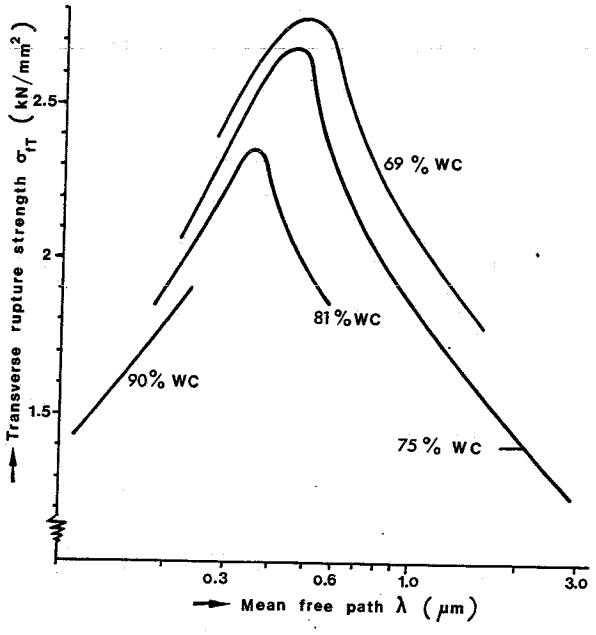

Fig. 1 Transverse rupture strength (σ_{fT}) as a function of mean free path for various compositions (Gurland and Parikh [1])).

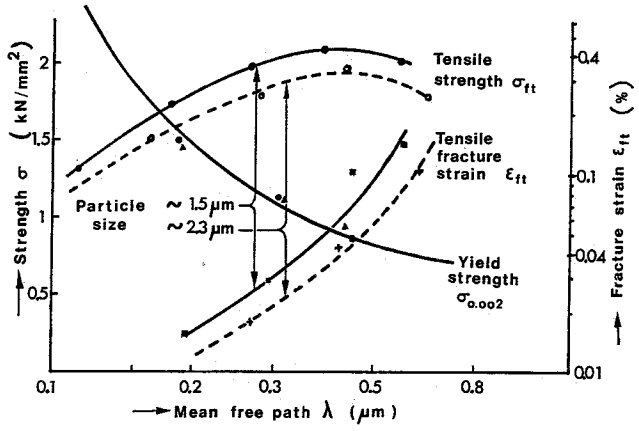

Fig. 2 The influence of grain size on tensile strength (σ_{ft}) and fracture strain (ε_{ft}) for straight carbides (Doi et al. [5])).

II The influence of the isostatic-stress component on brittle failure.

It has been observed on a number of occasions that strength of materials is a function of the isostatic-stress component. Brandes [3]) showed that fracture strength in uniaxial tension can be formulated as

$$\sigma_{ft} = R_o + (1 - 2\nu)p \qquad (2)$$

where σ_{ft} is the tensile strength, R_o is the strength related to p=0 and p stands for the isostatic stress. This isostatic-stress dependency is particularly pronounced for brittle materials. Recently, Shaw et al. [6]) reported similar effects for cemented carbides. The extent of the influence of isostatic stress was found to depend on the cobalt content of the specimen; the lower the percentage of cobalt the larger the effect. In these cases, the value of the isostatic-stress component was taken as the average value of the principal bulk stresses.
Consideration of the bulk stress field only has to date, however, not led to an explanation of the difference in isostatic-stress dependency on failure for carbides of different cobalt content. This might yet be possible if we consider the local stresses. Assuming brittle fracture to be preponderantly caused by the inability for stress relaxation by plastic deformation in the binder phase, it seems rewarding, in the above context, to examine the relation between brittle failure and the ratio of effective stress and maximum tensile stress in the binder, $\bar{\sigma}/\sigma$.

III Structural parameters and their influence on the stress distribution in the binder phase of cemented carbides.

Bridgman [6]) noticed that when performing tensile tests involving a high degree of plastic flow, the state of stress in the necking area can no longer be considered uniaxial. Applying the model of Fig. 3a, which shows a toroidal-shaped reduction area characterized by the ratio R/h and assuming a three dimensional state of stress, Bridgman derived the relation

$$\bar{\sigma}/\bar{\sigma}_z = c_B = \left[\left(1 + \frac{2h}{R}\right)\ln\left(1 + \frac{R}{2h}\right)\right]^{-1} \qquad (3)$$

This relationship explains the results of tensile tests at high strain values ($\bar{\sigma}$ stands for the effective stress, whilst $\bar{\sigma}_z$ represents the average value of the axial tensile stress related to the true area). The factor c_B is known as the Bridgman factor.

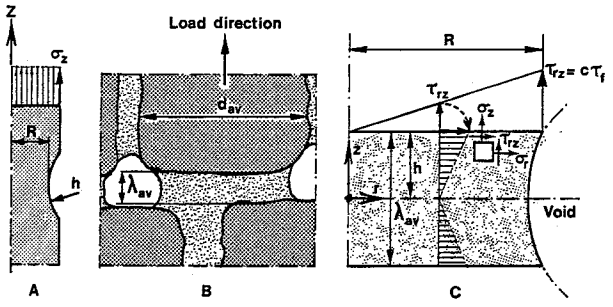

Fig. 3 a) Geometry of the Bridgman model.
b) Analogue for the structure of cemented carbides.
c) Idealisation and stress distribution of the analogue model.

The graphical representation of Eq. (3) is given as the solid line in Fig. 4. The curve shows that high values of R/h result in small values of c_B, meaning that the value of the effective stress $\bar{\sigma}$-relative to σ_z- is small. Under critical load conditions the possibility for plastic-flow relaxation should then be small, with a subsequent high risk of brittle failure.
Close examination of the structure of cemented carbides reveals, both on the surface and in the bulk (particularly in and around voids and pores) specific detail that is geometrically comparable to the tensile test situation of Fig. 3[a]. It seems therefore justified to adopt the analogue model of Fig. 3[b], where it will be noticed that $d_{av}/2$ substitutes for R, whilst half the average value of the mean free path $\lambda_{av}/2$ represents a fair minimum value of the radius. Generally, the ocurrence of intergranular voids is less frequent than is suggested in Fig. 3[b]. Putting the average effective distance between the voids equal to kd_{av}, an expression analogous to Eq. (3) is arrived at :

$$\left(\frac{\bar{\sigma}}{\sigma_z}\right)_{z=0} = c = \left[\left(1 + \frac{2\lambda_{av}}{kd_{av}}\right)\ln\left(1 + \frac{kd_{av}}{2\lambda_{av}}\right)\right]^{-1} \qquad (4)$$

The factor k depends upon the density of the voids. Its value will be largely determined by specific material processing conditions. The ratio d_{av}/λ_{av} is a structural parameter and will be characteristic for a specific grade. The potential significance of this parameter to failure, in terms of the ultimate uniaxial strain, is shown in Figs. 5 and 6.

It can be noticed that both figures no longer differentiate on the basis of grain size. The data of Fig. 6 deals with a number of different commercial carbides; the solid lines represent cobalt bonded types of two different manufacturers whilst the dotted line relates to the molybdenum-nickel bonded types for either straight or alloyed grades. Fig. 6 suggests that the slopes of the different lines are equal. More data are required, however, to confirm this. The difference in offset between the cobalt lines in Figs. 5 and 6 may be due to the specific processing and test methods used. For instance, in the tensile test (Fig. 5) each unit volume material is uniformly and equally loaded. This is not the case in the bending test. (Fig. 6).

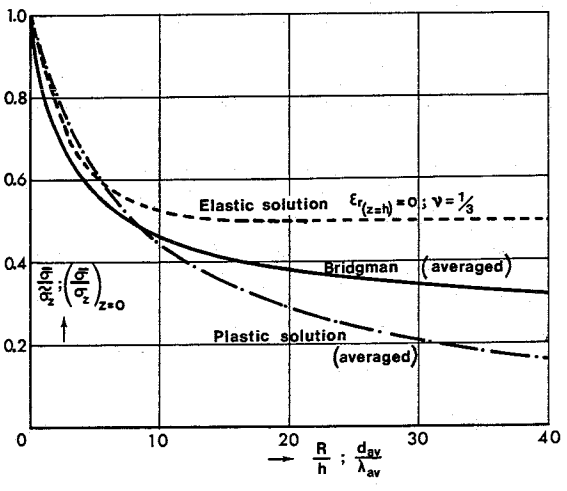

Fig. 4 The Bridgman factor as a function of the ratio R/h and the corresponding upper and lower bound solutions for cemented structures vs. d/λ.

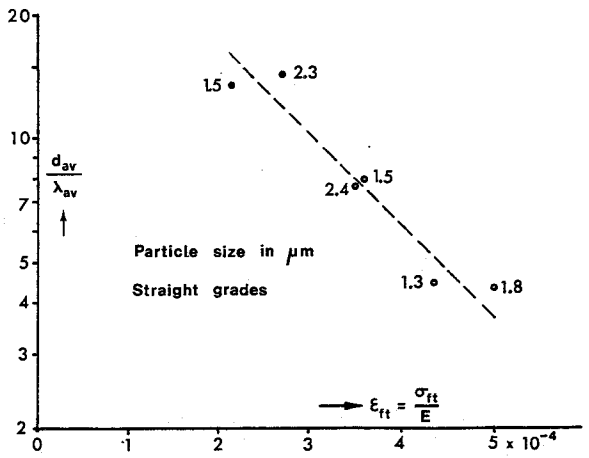

Fig. 5 The ultimate uniaxial strain (ε_{ft}, tensile test) as a function of d_{av}/λ_{av} (Data from Fig. 2).

This results in lower tensile strength values. Experience with brittle materials also indicates that tensile test results are less reliable than those from bending tests. A differentiation between cobalt grades will no longer be present when effects due to processing, such as porosity, are taken into account via the E-modulus (See further Section 4). One can therefore not expect singularity in terms of d/λ and ε_f for the data of Figs. 5 and 6.

The ultimate uniaxial strain can thus be formulated as

$$\varepsilon_f = A - B.\ln(d_{av}/\lambda_{av}) \qquad (5)$$

where A and B are constants, specific values depending on the type and state of the binder layer and test load characteristics. The value of the parameter d_{av}/λ_{av} for cemented carbide cutting tools varies between 10 and 50, while it seems reasonable to

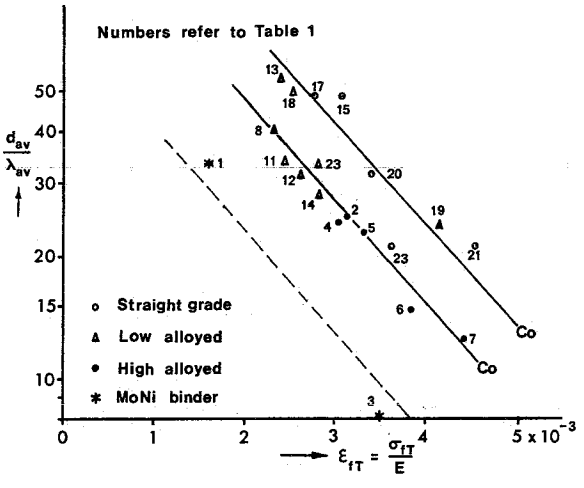

Fig. 6 The ultimate uniaxial strain (ε_{fT}, bending test) vs. the ratio d_{av}/λ_{av} for a number of commercial grades (Table 1).

accept that the value of k substantially exceeds 1. Realizing this, we use the next approximations

$$1 + \frac{2\lambda_{av}}{kd_{av}} \approx 1 \qquad (6)$$

$$1 + \frac{kd_{av}}{2\lambda_{av}} \approx \frac{kd_{av}}{2\lambda_{av}} \qquad (7)$$

Introducing this into Eq. (4) we get

$$c \approx \ln^{-1}\left(\frac{kd_{av}}{2\lambda_{av}}\right) \qquad (8)$$

Combining the Eqs. (8) and (5), we are able to express the maximum uniaxial strain directly in terms of the specific state of stress.

The use of the tensile test analogue (Fig. 3) to our problem gives rise to the following reservations. Firstly, unlike the necking phenomenon in a tensile specimen, the plastic flow in the carbide intergranular layer is localized and concentrated in the immediate vicinity of the voids. Secondly, the Bridgman factor has not been verified for values of R/h exceeding 10, this being a definite maximum value for the tensile test. Cemented carbide structures, however, show values of d_{av}/λ_{av} up to 50, which means that even for k=1 certain approximations made by Bridgman may no longer be allowed. The next analysis therefore provides for an independent upper (elastic) and lower (plastic) bound solution for the ratio $\bar{\sigma}/\sigma_z$ in the intergranular binder layer, the results of which appear to justify the initial use of the Bridgman factor in relating the state of stress (c) to the ultimate uniaxial strain. The elastic solution has been derived while limiting the maximum shear stress τ_{rz} at the location r=R, z=h, (Fig. 3c) to $c\tau_f$ (τ_f stands for the flow shear stress, while c<1). A suitable solution of the stress distribution in the layer has been obtained by using a fifth degree stress polynominal. This polynominal combines two fifth degree and two third degree stress polynominals as develloped by Timoshenko [7] for the derivation of stress fields in circular plates. This procedure ensures that the requirements concerning equilibrium and compatibility are being met. The following boundary conditions have been set (Fig. 3c).

$$\text{For } r = R \begin{cases} \tau_{rz} = c\tau_f; \; c<1 \\ \sigma_r = 0 \end{cases}$$

and for $z = h$: $\varepsilon_r = 0$ (i.e. an infinitely high E-value of the grains)

The derivation of the different formulae representing the stress distribution is given in Appendix I, from which results

$$\tau_{rz} = \frac{c\tau_f}{Rh} rz \qquad (9)$$

$$\sigma_r = \frac{c\tau_f}{2Rh}(5z^2 + R^2 - r^2) \qquad (10)$$

$$\sigma_z = \frac{c\tau_f}{Rh}(6h^2 - z^2 + R^2 - r^2) \qquad (11)$$

From this follows for the stress ratio in the middle of the layer (z=0) :

$$(\bar{\sigma}/\sigma_z)_{z=0} = \frac{R^2 - r^2 + 12h^2}{2(R^2 - r^2) + 12h^2} \qquad (12)$$

For r=R, at the void surface, the state of stress is uniaxial. With respect to brittle fracture the worst condition is reached at the centre of the layer where

$$(\bar{\sigma}/\sigma_z)_{\substack{z=0,\\ r=0}} = \frac{(R/h)^2 + 12}{2(R/h)^2 + 12} \qquad (13)$$

This relation is depicted in Fig. 4 as the dotted line.
As to the plastic solution, the elastic shear stress distribution given in Eq. (9) has once more been adopted. This seems reasonable since plastic deformation up to failure is highly localized in the immediate vicinity of voids and pores. Further assuming $\bar{\sigma}=2\tau_f$ for z=0, one arrives at the equation (see appendix II)

$$(\bar{\sigma}/\sigma_z)_{z=0} = \frac{1}{(R/8h) + 1} \qquad (14)$$

This relation is depicted in Fig. 4 as the chain-dot line. Just like the Bridgman solution, the expression of Eq. (14) concerns the average value of the ratio $\bar{\sigma}/\sigma_z$. The elastic solution (Eq. (13)) is limited to the location z=0, r=0, i.e. the most dangerous location in the layer. Considering the different solutions shown in Fig. 4, it may be expected that the Bridgman factor will best quantify the ratio $\bar{\sigma}/\sigma_z$. A fundamental relation between this ratio and the ultimate uniaxial strain has, however, not yet been succesfully derived. It is suggested that future effort be putinto this subject.

IV Fracture toughness and its relation to Young's modulus.

The value of the ratio d_{av}/λ_{av} depends predominantly on the percentage of bindermaterial. Factors such as shape and size distribution of the particles are not expected to have any significant influence on the value of this ratio [8]. For cubic grains of uniform size - which resemble the actual shape of tungsten carbide grains - one can derive that

$$d_{av}/\lambda_{av} = \frac{X_f}{1 - X_f} \qquad (15)$$

where $X_f = \sqrt[3]{1-f}$ and f is the volume fraction of the binder. The

Grade (ISO-code)	Number	Make	E (10^5 N/mm^2)	σ_{fT} (10^3 N/mm^2)
P01	1	A	4.50	0.70
P10	2	A	4.90	1.50
	3	D	4.27	1.55
P20	4	A	5.30	1.60
P30	5	A	5.20	1.70
P40	6	A	5.50	2.10
P50	7	A	5.05	2.20
K01	8	A	6.65	1.50
	9	B	6.41	1.59
	10	D	6.62	1.38
K10	11	A	5.80	1.40
	12	A	6.50	1.70
	13	D	6.52	1.59

Grade (ISO-code)	Number	Make	E (10^5 N/mm^2)	σ_{fT} (10^3 N/mm^2)
K20	14	A	6.40	1.80
	15	B	6.48	2.00
	16	C	6.61	1.76
	17	D	6.48	1.79
	18	D	6.48	1.66
K30	19	C	5.49	2.28
	20	D	6.07	2.07
	21	D	5.45	2.48
K40	22	B	5.44	2.69
M20	23	A	6.10	1.70
	24	B	6.48	1.86
M40	25	A	6.20	2.20
91/9	26	B	6.00	2.34
90/10	27	B	6.00	2.41

Table 1

Specifications of the cemented carbides of Figs. 6 and 7 (The numbers refer to the specific position in the Figures).

E-value also depends very much on the fraction of binder material. From results of Rüdiger et al.[9], dealing with straight grades within the range 5 < vol. % cobalt < 40, one can derive that the E-value in N/mm^2 can be calculated from

$$E = 700 - 662.f \quad (N/mm^2) \qquad (16)$$

The numerical values given in Eq. (16) do of course result from the specific sampling and as such will restrict the use of this relation in a general sense. As an example, the lower solid line of Fig. 6 can be expressed as

$$\varepsilon_{fT} = (8.75 - 1.75\ln(d_{av}/\lambda_{av}))10^{-3} \qquad (17)$$

The Eqs. (15), (16) and (17) can be rearranged to yield

$$\varepsilon_{fT} = \left\{8.75 - 1.75\ln\left[\left(\sqrt[3]{1 - \frac{7.00 - E.10^{-5}}{6.62}}\right)^{-1} - 1\right]^{-1}\right\}10^{-3} \qquad (18)$$

Such equations enable us to determine fracture toughness as expressed by uniaxial strain when only the E-modulus is known. Fig. 7 demonstrates, for a number of commercial K- and M-grades (with percentages of TiC, TaC etc., smaller than 3 %), that the calculated ε_{fT}-values (Eq. (18)) are in fair agreement with the original σ_{fT}/E-values. It is a fact that, notwithstanding a high sensitivity of ε_{fT} (Eq. (18)) to specific E-values (relative-error amplification up to 10), a differentiation in cobalt bonded grades (Fig. 6) no longer occurs. Evidently, ε_{fT} is not uniquely dependent on d/λ. Most likely one has to consider the contribution of k (porosity) which has been left out in Fig. 6. This is in principle done via Eq. (18) in Fig. 7, where the experimentally obtained E-values selectively account for the influence of porosity. In this respect, the numerical values of Eq. (16) appear to represent an acceptable mean, which in the same context also holds for the values chosen for A and B in Eq.(17). It turns out that Eq. (18) no longer holds when substantial amounts of titanium and tantalum carbides are present, or in general, when the carbide size distribution is distinctly non uniform. This is particularly the case for the low numbered K- and P-grades. The deviations are believed to be caused by the character of Eq. (16).

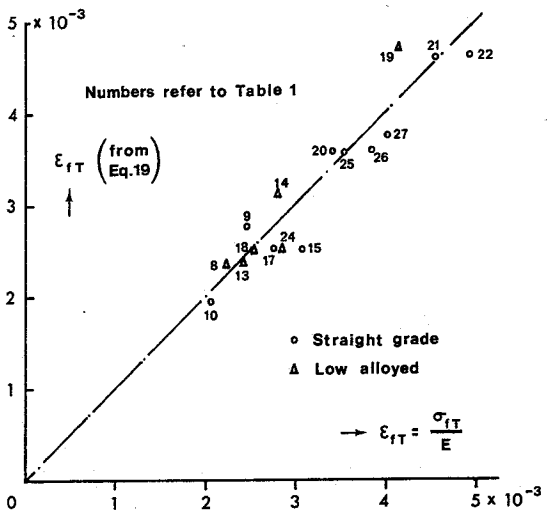

Fig. 7 Comparison between the calculated ultimate uniaxial strain (Eq. (18)) and the original σ_{fT}/E-value (TiC-TaC < 3 %).

V Conclusions

Fracturing in cemented carbides is controlled by the type of binder, the structural parameter d_{av}/λ_{av} and the degree of porosity. It has been found that the ultimate uniaxial strain - an adequate toughness criterion - is related to the ratio d_{av}/λ_{av}. A possible explanation for this behaviour follows from the fact that an increase of d_{av}/λ_{av} results in a decrease of the ratio effective stress to relevant tensile stress ($\bar{\sigma}/\sigma$), ultimately leading to an increased risk of failure.
When for the various types of structure the expression E=E(f) is known, one may arrive at an equation which permits the prediction of failure from the E-value. The influence of porosity will then be automatically included. It has been shown that this procedure is valid for most K- and M-grades, for which the ultimate uniaxial strain can be calculated with Eq. (18). This equation no longer holds for alloyed grades. It is believed that this is due mainly to the non-uniformity of particle size. These grades therefore require expressions other than Eq. (16).

Acknowledgement

The authors wish to thank Dr. J.A.H. Ramaekers for the discussions and suggestions made on the subject of stress fields in the binder layer.

References

1. Liebowitz, H., Fracture, Vol. III, Academic Press (1972).
2. Hatano, T., Int. J. of Fracture Mechanics, Vol. 5, 1(1969)73.
3. Brandes, M., Int. J. of Fracture Mechanics, Vol. 1, 1(1965)56.
4. Kals, H.J.J., Veenstra, P.C., Proposal for cooperative research on testing and classification of cemented carbide tool materials, Report WT 0333, Eindhoven University of Technology, presented at the meeting of the STC-"Toughness", C.I.R.P., Kyoto, aug. 1974.
5. Doi, H., Fujiwara, Y., Oosawa, Y., Proc. of the Int. Conf. on Mech. Behaviour of Materials, Kyoto, Vol. V (1972) 209.
6. Bridgman, P.W., Trans. Am. Soc. Metals, 32(1943)553.
7. Timoshenko, S., Goodier, J.N., Theory of Elasticity, McGraw-Hill Book Company. 1951.
8. Fullman, R.L., Trans. AIME, J. of Metals, March (1953)447.
9. Rüdiger, O., Ostermann, G., Kolaska, H., Techn. Mitt. Krupp. Forsch-Ber. Band 28, 2(1970)33.

Appendix I

An appropriate stress polynominal is found in (see reference 7, pp. 348 and 349).

$$\phi = A\left[z^5 - \frac{10}{9}z^3(r^2 + z^2) + \frac{5}{21}z(r^2 + z^2)^2\right] +$$

$$+ B(2z^3 - 3r^2z)(r^2 + z^2) + Cz(r^2 + z^2) + Dz(2z^2 - 3r^2)$$

The expressions for the stresses follow from the equations

$$\sigma_r = \frac{\partial}{\partial z}\left(\nu\nabla^2\phi - \frac{\partial^2\phi}{\partial r^2}\right)$$

$$\sigma_z = \frac{\partial}{\partial z}\left[(2 - \nu)\nabla^2\phi - \frac{\partial^2\phi}{\partial z^2}\right]$$

$$\tau_{rz} = \frac{\partial}{\partial r}\left[(1 - \nu)\nabla^2\phi - \frac{\partial^2\phi}{\partial z^2}\right]$$

By substituting ϕ, adjusting the constants so as to satisfy the boundary conditions (see Fig. 3c)

$$\left.\begin{aligned}\tau_{rz} &= c\tau_f \;;\; c \leqslant 1\\ \sigma_r &= 0\end{aligned}\right\} \text{ for } r = R$$

$$\varepsilon_r = 0 \quad \text{for } z = h$$

and putting $\nu = 1/3$, one arrives at the equations (9), (10) and (11) in section III.

Appendix II

Departing from the elastic shear stress distribution

$$\tau_{rz} = \frac{\tau_f}{Rh} rz$$

we use the first of the equations of equilibrium, which by virtue of the rotatory symmetry can be written as

$$\frac{\partial\sigma_r}{\partial r} = -\frac{\partial\tau_{rz}}{\partial z}$$

It follows that

$$\sigma_r = -\int\frac{\tau_f r}{Rh}\,dr = -\frac{\tau_f r^2}{2Rh} + C$$

Realizing that $\sigma_r = 0$ for $r = R$ one arrives at the equation

$$\sigma_r = \frac{\tau_f}{Rh}(R^2 - r^2)$$

According to Huber Hencky - von Mises one can write under the given circumstances

$$\bar{\sigma} = (\sigma_z - \sigma_r)_{z=0}$$

Taking for $z = 0$ the condition $\bar{\sigma} = 2\tau_f$, it follows that

$$(\sigma_z)_{z=0} = \tau_f\left[\frac{1}{2Rh}(R^2 - r^2) + 2\right]$$

and hence for the lower bound solution as mentioned in section III :

$$\left(\frac{\tilde{\sigma}_z}{\bar{\sigma}}\right)_{z=0} = \frac{2\pi}{\pi R^2}\int_0^R\left\{\frac{1}{2Rh}(R^2 - r^2) + 2\right\}rdr = \frac{R}{8h} + 1$$